Drosophila Circadian Rhythms: Stability Robustness Analysis and Model Reduction

Jorge M. Gonçalves
University of Cambridge
Department of Engineering
Cambridge CB2 1PZ, UK
jmg77@cam.ac.uk
www.eng.cam.ac.uk/∼jmg77/

Tau-Mu Yi
University of California at Irvine
Developmental and Cell Biology
Irvine, CA 92697-2300, USA
tmy@uci.edu
yilab.bio.uci.edu/

Abstract

This paper shows how biological oscillations can be rigorously analysed using several analysis tools from the field of control and dynamical systems theory. Testing for local stability of the periodic orbit provides information about the system close to the limit cycle. It determines which modes of the system are harder or easier to control and may lead to a simplification of the model. Local stability, by definition, does not guarantee stability further away from the limit cycle. However, the approximation of nonlinear models by piecewise linear systems can be used to determine more global robustness properties of the system. To illustrate these ideas, this paper investigates two models of circadian rhythms in *Drosophila*: one by Gonze et al. and a more generic model by Vilar et al. that describes the biological clock in *Drosophila* as well as other organisms. For both models, local stability analysis shows that most small perturbations to initial conditions around the limit cycle disappear after one cycle (24 hours). In addition, we demonstrate that in each model only two modes are relevant. Thus both models can be reduced to third-order systems, and the direction of the excitable modes identify the disturbances which can cause the most harm. Analysing the piecewise linear approximation of the Gonze-Goldbeter model reveals large regions of stability around the limit cycle, which confirms the linear analysis results and offers further insight into the source of robustness in these systems. In summary, the tools described in this paper should help characterise the mechanisms underlying the control and regulation of circadian rhythms and other limit cycle behaviours.

1 Introduction

Many aspects of the physiology of living organisms (e.g., body temperature, wake-sleep cycle, etc.) oscillate with a period of approximately 24 hours, corresponding to the length of a day. These circadian rhythms are remarkable for their robustness to external and internal disturbances [2, 16]. Experiments have uncovered the molecular basis for the clock underlying these rhythms in several organisms from the fungus *Neurospora* [3] to *Drosophila* (the common fruit fly) [17] to mammals [15]. Simulations of mathematical models constructed from these data reproduced key characteristics of the oscillations [4, 12], but a more in-depth understanding has been impeded by the complexity of the models and the challenge of rigorous robustness analysis.

Figure 1 represents a simplified mechanism for producing circadian rhythms in *Drosophila* [8, 9]. Two main cycles, one regulatory and one autocatalytic, maintain the system with an extremely robust periodicity close to 24 hours. Two genes *per* and *tim* are transcribed and translated into the proteins PER and TIM which will then form the PER-TIM complex. This complex enters

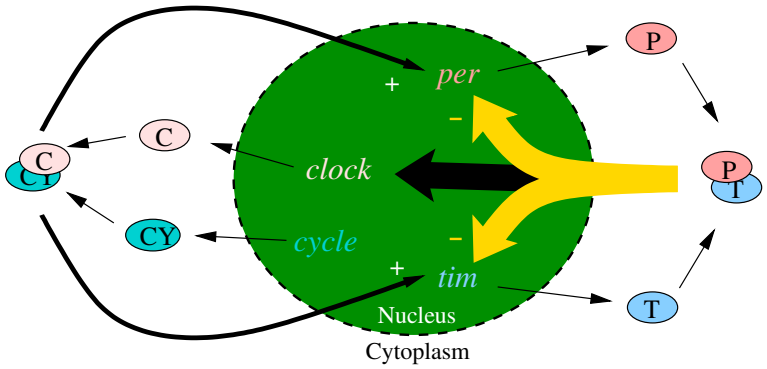

Figure 1: Circadian rhythms in *Drosophila* [8, 9], showing the negative feedback loops (yellow) and the positive feedback loops (red).

the nucleus and inhibits the transcription of both *per* and *tim* genes. This is the main regulatory negative feedback loop. As both PER and TIM concentrations increase, the complex activates the transcription of the gene *clock* which is transcribed and translated into the CLOCK protein. CLOCK then binds with CYCLE and this complex activates both *per* and *tim*, forming a positive feedback loop.

This paper introduces rigorous tools from control theory to gain new insights into how circadian rhythms work, and to better understand the source of robustness of such systems. To illustrate these tools, we investigated two models of *Drosophila* circadian rhythms, one devised by Gonze, Goldbeter and colleagues [7], and another more generic model by Vilar and colleagues [1].

This paper is organised as follows. Section 2 analyses the model by Gonze et al. [7] and section 3 analyses the model by Vilar et al. [1]. Both sections include subsections on the analysis of each model. First, the Poincaré map is linearised to determine which modes dominate the system close to the limit cycle, and to help reduce the models. Then, one of the models (Gonze-Goldbeter) is approximated by a piecewise linear system which can be analysed to conclude about more global robustness properties. Conclusions can be found in Section 4. The Appendix contains more detailed descriptions of both models, and several previously published technical results are reprised for the sake of completeness.

2 Model with regulatory feedback

A schematic description of the Gonze-Goldbeter model [7] is provided on the left of Figure 2. This model captures the negative feedback loop between genes *per* and *tim* and their associated proteins PER and TIM in Figure 1, but not the positive feedback. It consists of 10 state variables, $[M_P\ P_0\ P_1\ P_2\ M_T\ T_0\ T_1\ T_2\ C\ C_N]$ (see Appendix A.1.1) that capture the dynamics of the PER and TIM proteins and the *per* and *tim* mRNAs. Simulations, seen on the right of Figure 2, show that the system has a limit cycle oscillation with a period of approximately $T^* = 24$ hours.

2.1 Linear analysis and model reduction

2.1.1 Poincaré maps

Analysis of oscillations in nonlinear or hybrid systems systems is typically done with the so-called *Poincaré map* (see, for example, [11]). Figure 3 shows an example of a limit cycle oscillation of some nonlinear system. Take a hyperplane S transversal to the limit cycle trajectory and let $x^* \in S$

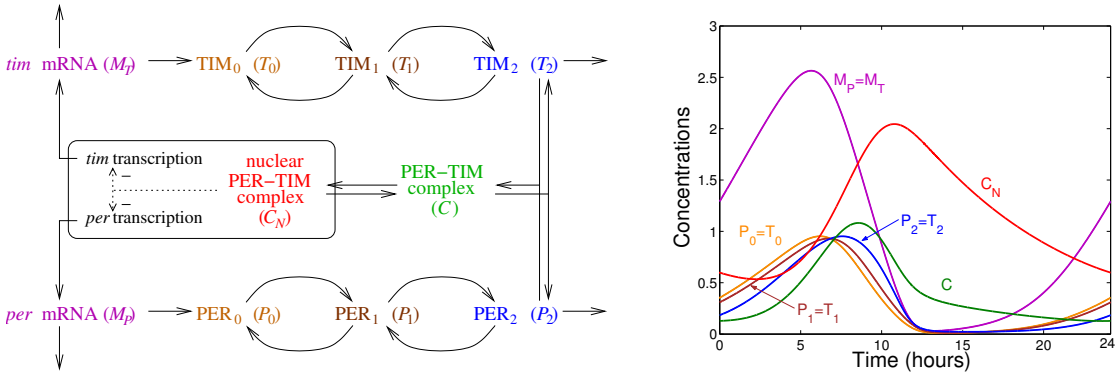

Figure 2: Model for circadian rhythms in *Drosophila* from [7] (left). Simulation showing the limit cycle oscillations (right).

be the intersection of the limit cycle with S. Then, take some initial condition $x_0 \in S$ in some local section containing x^*. The Poincaré map is defined as the map from x_0 to the return of the trajectory to x_1 also in that local section in S. Basically, a Poincaré map reduces the study of an n-dimensional system to a discrete $n-1$-dimensional system in a manifold. The idea is to check whether the distance from x_1 to x^* is smaller than the initial distance from x_0 to x^*. This would show that the Poincaré map is contracting, and thereby proving stability properties of the original limit cycle trajectory.

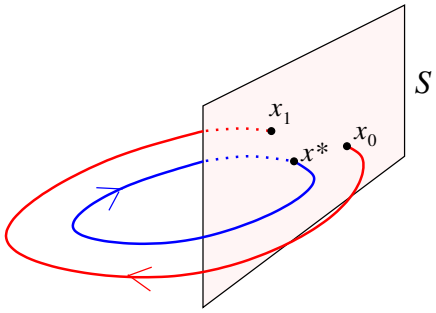

Figure 3: Limit cycle oscillation and Poincaré maps.

The problem with Poincaré maps is that, in general, they cannot be found explicitly and are typically nonlinear, multivalued, and not continuous. However, it is possible to study linearisations of Poincaré maps [13] and to analyse Poincaré maps for piecewise linear systems [6, 5]. We start with linear analysis of Poincaré maps of the Gonze-Goldbeter model.

2.1.2 Linearisation of Poincaré maps

Poincaré maps can be linearised using the results from [13]. For completeness, those results are reproduced in Appendix B. Denote P as the Poincaré map from some transversal surface S to S, and DP as the Jacobian of the Poincaré map.

The only nonzero eigenvalues of the matrix DP for the Gonze-Goldbeter model are $\lambda_1 = 0.0000452$ and $\lambda_2 = 0.000000201$. This shows that limit cycle is locally stable and that the rate of convergence after a complete cycle of any initial condition close enough to the limit cycle is extremely fast. It also shows that only two states of the Poincaré map are interesting. The others states of the linearised

map return to the limit cycle just after one cycle.

This results also shows where the system is most vulnerable (i.e., which initial conditions close to the limit cycle give rise to the largest disturbances). The corresponding eigenvectors associated with λ_1, λ_2 in $\Phi_{T^*}(x^*)$ (the linearised transition matrix along the limit cycle, defined in Appendix B) are:

$$v_1 = \begin{pmatrix} 0.5417 \\ 0.1973 \\ 0.2186 \\ 0.2558 \\ 0.5417 \\ 0.1973 \\ 0.2186 \\ 0.2558 \\ 0.1498 \\ -0.2939 \end{pmatrix} \qquad v_2 = \begin{pmatrix} -0.2417 \\ -0.1000 \\ -0.1685 \\ -0.6349 \\ 0.2417 \\ 0.1000 \\ 0.1685 \\ 0.6349 \\ 0 \\ 0 \end{pmatrix} \tag{1}$$

Notice that a close enough initial condition to the limit cycle along an eigenvector of $\Phi_{T^*}(x^*)$ will result in a trajectory that only excites the associated mode.

The first mode is of greater interest since it is associated with the largest eigenvalue. A closer look at v_1 reveals that entries 1 to 4 are point-wise equal to entries 5 to 8. Thus, the circadian clock is maximally perturbed when the concentrations of M_P, P_0, P_1, P_2 are perturbed the same way as the concentrations of M_T, T_0, T_1, T_2, in the appropriate relation given by entries 1 to 4 and with C and C_N also with the appropriate relation given by the last two entries in v_1. In other words, the worst perturbation is along the same (or opposite) direction of v_1.

In the second mode, entries 1 to 4 are point-wise symmetric to entries 5 to 8. Thus, the second mode is optimally excited when the concentrations of M_T, T_0, T_1, T_2 are perturbed symmetrically when compared with the concentrations of M_P, P_0, P_1, P_2, in the appropriate relation given by entries 1 to 4 and with C and C_N not perturbed.

Since any small perturbation Δ to the system at x^* can be written as a linear combination of the eigenvectors v_i of $\Phi_{T^*}(x^*)$, i.e., $\Delta = \alpha_1 v_1 + \cdots + \alpha_n v_n$, any perturbation to the limit cycle at x^* such that $\alpha_1 = \alpha_2 = 0$ results in trajectories that return to the limit cycle just after one cycle.

2.1.3 Model reduction

For small perturbations around the limit cycle, only two states are of interest. Thus, the Poincaré map close to the limit cycle can be reduced to a 2nd-order system. Let $V = [v_1 \cdots v_n]$ and $\Lambda = \text{diag}(\lambda_1 \cdots \lambda_n)$ be the eigenvectors and eigenvalues of DP, respectively. Using the notation from Appendix B, define

$$W = I - \frac{1}{Cf(x^*)} f(x^*) C$$

Then, $DP = W\Phi_{T^*}(x^*)$ and $\Lambda = V^{-1} DP\, V$. In the V basis, the reduced second order system is

$$\begin{cases} x_1[t+1] &= 0.0000425 x_1[t] \\ x_2[t+1] &= 0.000000201 x_2[t] \end{cases}$$

with initial condition $x[0] = x_0$, where $x = (x_1 \quad x_2)'$. These two states are associated with v_1 and v_2, respectively. Perturbing first state x_1 is equivalent to perturb the original system along the direction of v_1. Similarly, perturbing the second state x_2 is equivalent to perturbing the original system along v_2.

2.2 Approximation by piecewise linear systems

Besides local stability, typically not much more can be said rigorously about stability and robustness of Poincaré maps. Recent results in piecewise linear systems (PLS), however, allow one to study the limit cycle behaviour of nonlinear systems approximated by PLS. In this section, we explore several such approximations to identify regions of stability around the limit cycle. A brief introduction to PLS is given in Appendix C.

The first step is to find an approximate PLS of the original nonlinear system. One approach is to approximate each nonlinearity in the system dynamics by piecewise linear functions. It should be noted that every nonlinearity can be arbitrarily well approximated by refining the piecewise linear functions.

A common nonlinearity in the Gonze-Goldbeter model and other biological models using Michaelis-Menten kinetics is the following (see Figure 4):

$$f(x) = \frac{x}{K+x} = \frac{1}{1+\frac{K}{x}}$$

There are clearly three regions: a linear region for small values of x, an intermediate region, and a saturated region for large x. If during a cycle, a nonlinearity associated with some concentration x has either only small or large values, then it can be approximated by a linear function or by a constant, respectively (see Figure 4). If x takes values in three regions then it can be approximated by a piecewise linear function as illustrated by two examples in Figure 4.

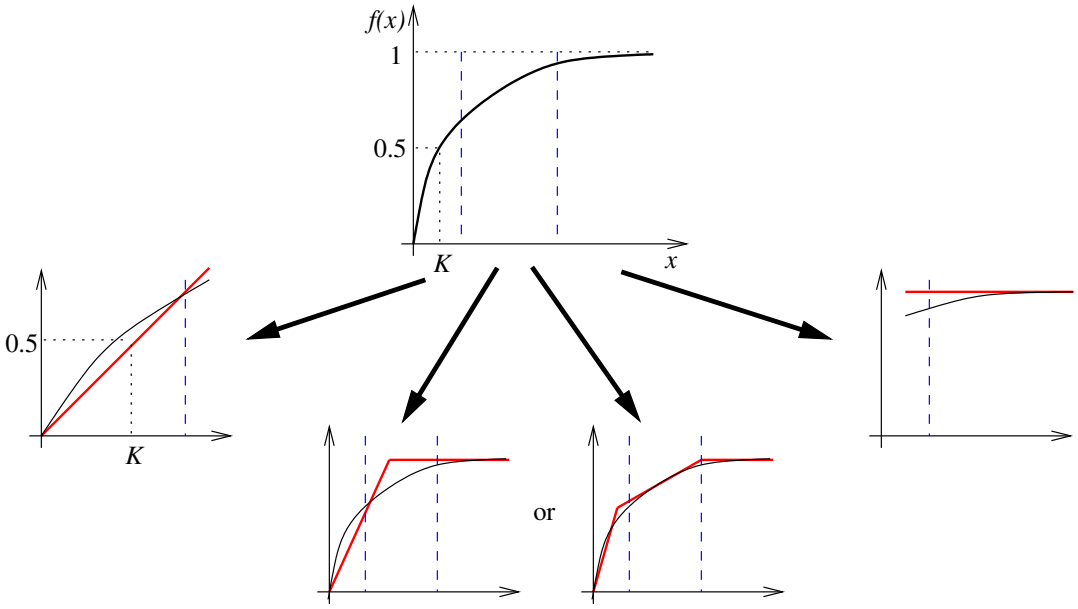

Figure 4: Nonlinearity and possible approximations depending on the range of x.

To illustrate these ideas, we study a simplified version of the circadian rhythm model from [7]. The limit cycle oscillations on the right of Figure 2 show how several concentrations have the same value: $M_P = M_T$, $P_0 = T_0$, $P_1 = T_1$, $P_2 = T_2$. A simplified model assumes that initial conditions of these concentration's pairs are equal. Due to the symmetry of the system, this guarantees that the pairs always vary in the same way, even away from the limit cycle oscillation. This reduces the model to a 6th–order system which can be found in Appendix A.1.2.

A special case of having the above concentration's pairs with equal initial conditions is when we study small enough perturbations (so that the linearisation holds) along the direction of eigenvector

v_1 in (1). As above, the above concentration pairs would have the same value for all time. Remember that v_1 is the direction associated with the highest eigenvalue of the linearised Poincaré map, the mode that takes longer to disappear and can cause more damage to the system.

By looking at the model in Appendix A.1.2 and the right of Figure 2, we can have an idea of the range of values each concentration has along one cycle. This allows to choose which type of approximation to use in Figure 4. For example, in the first nonlinearity of the differential equation dP_2/dt, $K_{3P} = 2$ and the range of values for P_2 along a cycle is approximately $[0\ \ 1]$. From Figure 4, this lead us to conclude that this nonlinearity is mostly in the linear regime, and can be approximated by a linear function. On the other hand, the nonlinearity involving the term $K_{dP} = 0.2$ goes from the linear region to the saturated regime. Thus, it requires a piecewise linear approximation as in the two examples in the middle of Figure 4.

For purposes of visualisation, in the following piecewise linear approximation of the simplified model in appendix A.1.2, the switches are employed with only two state variables: M_P and P_2. This allows us to visualise the PLS system projected into the subspace of dimension 2 consisting of the state variables M_P and P_2 (see the right side of Figure 5).

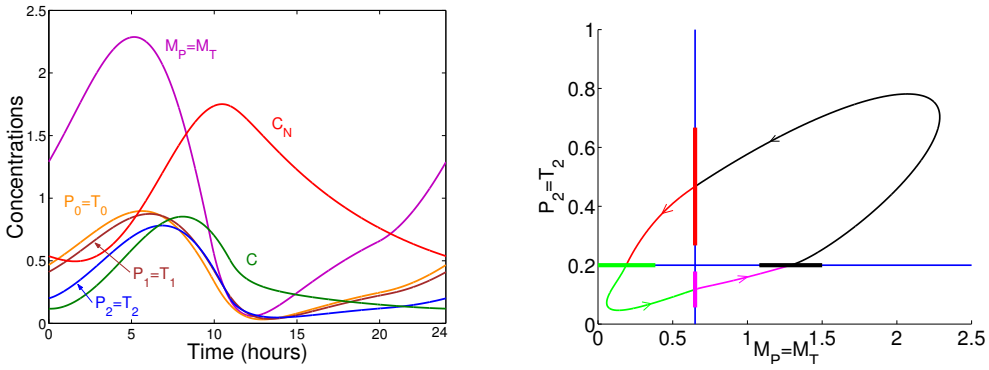

Figure 5: Approximation of the simplified model by a piecewise linear system: limit cycle oscillation (left); and limit cycle in the state-space projected into the 2nd dimensional subspace of state variables M_P and P_2 (right).

The left side of Figure 5 shows the limit cycle oscillations for the PLS model. When compared with the limit cycle oscillations of the original model on the right of Figure 2, both plots seem similar in terms of the trajectories of the various variables, which suggests that the approximation is reasonable.

The right side of Figure 5 shows the limit cycle projected into the two–dimensional subspace of the state variables M_P and P_2. Since these are the only two variables that have associated nonlinearities with switches, this two–dimensional subspace shows the four regions in which the state–space is divided: four linear systems divided by hyperplanes. The limit cycle intersects all of the four regions.

As in nonlinear systems, local stability of limit cycles of PLS can be easily checked. However, local stability only gives us information about the system in an arbitrarily small neighbourhood around the limit cycle. Using the results from [5], we were able to characterise regions of stability around the limit cycle for the PLS approximation. The right side of Figure 5 shows such regions of stability: at every intersection of the limit cycle with a switching surface, there is a thicker region on the switching surface that guarantees any trajectory starting in that region converges asymptotically to the limit cycle. As Figure 5 shows, this region is reasonably large which confirms our assumptions (mostly derived from simulation) that the system is robust.

As we change system parameters or the system network structure, this tool allows us to see how this region changes. This information may help explain what parameter or part or structure of the network is responsible for the robustness that is known to prevail in circadian rhythms.

3 Model with both regulatory and autocatalytic feedback

A schematic description of the Vilar model [1] is provided on the left of Figure 6. This model differs from from the Gonze-Goldbeter model in that it captures both the negative feedback loop and the positive feedback loop introduced in Figure 1. The model involves two genes: an activator A and a repressor R, which are transcribed into mRNA and subsequently translated into protein. The activator A binds to the A and R promoters, which increases their transcription rate. Thus, A acts as a positive feedback in transcription. On the other hand, R acts as a regulatory (negative) feedback by binding with A (to produce an inactive complex C) reducing activity of the activator A (see Figure 6). The model consists of 7 state variables $[D'_A\ D'_R\ M_A\ A\ M_R\ R\ C]$ and can be found in Appendix A.2.

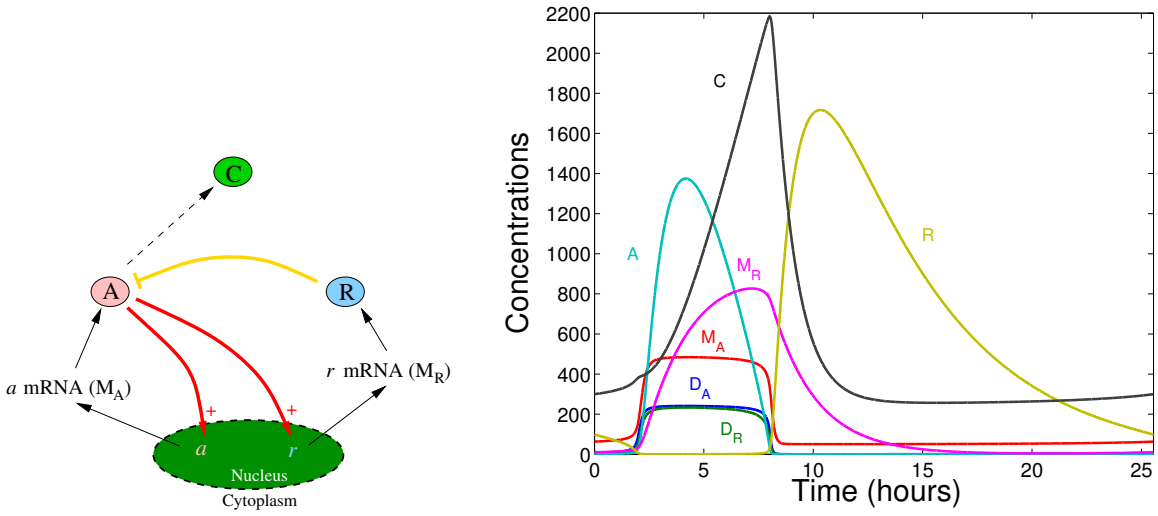

Figure 6: Model for a generic circadian oscillator [1] (left); Simulation showing the limit cycle oscillation (right—in this plot, the concentrations of D_A and D_R were scaled by 250, and M_A and M_R by 10 for purposes of visualisation).

This model slightly differs from the system in Figure 1 since it represents a generic genetic oscillator. The most basic differences are the facts that the repressor R represents both proteins PER an TIM, R does not regulate itself directly, and A activates itself. Simulations of this model, seen on the right of Figure 2, show that the system has a limit cycle oscillation with a period of approximately $T^* = 25$ hours.

3.1 Linear analysis and model reduction

As in Section 2.1.2, the Poincaré map associated with the limit cycle can be linearised. Here, the only nonzero eigenvalues of the matrix DP are approximately $\lambda_1 = 0.00000322$ and $\lambda_2 = 0.00000000686$. This shows that limit cycle is locally stable and that the rate of convergence after a complete cycle of any initial condition close enough to the limit cycle is extremely fast. In fact, the

largest eigenvalue of the system is over 10 times smaller than the largest eigenvalue of the model in [7], showing that locally this model converges faster to the limit cycle than the Gonze-Goldbeter model.

Again, only two states of the Poincaré map are interesting. The others states of the linearised map return to the limit cycle just after one cycle. The directions associated with the above eigenvalues are, respectively,

$$v_1 = \begin{pmatrix} 0.000278 \\ 0.000143 \\ 0.0127 \\ 0.0148 \\ 0.082 \\ -0.714 \\ 0.695 \end{pmatrix} \qquad v_2 = \begin{pmatrix} 0.000122 \\ 0.0000628 \\ 0.00582 \\ 0.00645 \\ -0.0675 \\ -0.307 \\ 0.949 \end{pmatrix} \tag{2}$$

These eigenvectors (associated with the only two nonzero eigenvalues) of the Jacobian of the Poincaré map, show that perturbations in both D'_A and D'_R have little effect in the system. Also, both eigenvectors reveal that the most destabilising concentrations are the concentrations of R and C. The first eigenvector v_1, associated with λ_1, is the most destabilising direction, since it is associated with the largest eigenvalue. This circadian clock is worst perturbed when the concentrations are perturbed with the proportion given by v_1. Similarly for v_2.

For small perturbations around the limit cycle, only two states are of interest. Following the same procedure as in Section 2.1.3, the Poincaré map close to the limit cycle can be reduced to the following 2nd-order system, in the V basis

$$\begin{cases} x_1[t+1] &= 0.00000322 x_1[t] \\ x_2[t+1] &= 0.00000000686 x_2[t] \end{cases}$$

with initial condition $x[0] = x_0$, where $x = (x_1 \quad x_2)'$. These two states are associated with v_1 and v_2, respectively. Perturbing first state x_1 is equivalent to perturb the original system along the direction of v_1. Similarly, perturbing the second state x_2 is equivalent to perturbing the original system along v_2.

This model reduction provides a reference for examining the accuracy of other attempts at model simplification. For example, in [1], the authors derive a nonlinear second order continuous model by focusing on the two slow variables R and C. Although the reduced linearised Poincaré map is 2nd-order (translating into a 3rd-order system in the original state-space), it is clear that $\lambda_2 << \lambda_1$ arguing that a first-order Poincaré map or 2nd-order state-space model can furnish a reasonable approximation. In addition, examining v_1 does indeed confirm that R and C are the two key variables which make the most significant contributions to the limit cycle behaviour. However, the above analysis also highlights limitations to the Vilar approximation, namely, excluding the minor mode v_2 and not taking into account variables such as M_R that exert a modest influence on the dynamics.

In the analysis above we have not performed any time-scale separation. Vilar et al. assume that the fast variables in the system (everything but R and C) are at quasi-steady-state so that their time derivatives are zero. We examined this assumption by plotting the time derivatives of the state variables during the progression of the limit cycle. Indeed, the derivatives were modest compared to dR/dt and dC/dt with the exception of dA/dt. Thus, setting $dA/dt = 0$ is not justified and could limit the accuracy of the approximation.

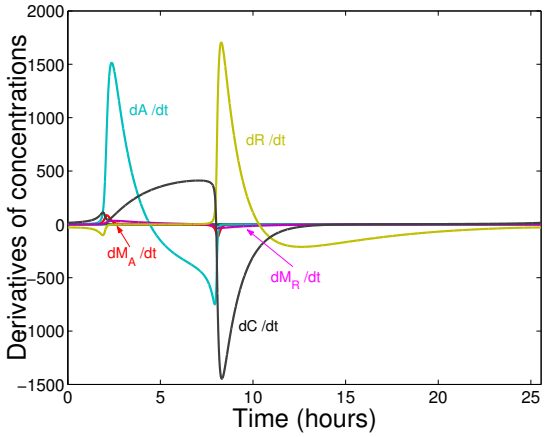

Figure 7: Derivatives of concentrations along the limit cycle oscillation for the model in [1].

4 Conclusions

The goal of this paper is to explain how oscillations can be analysed via linearisation of the Poincaré map and approximating the nonlinear dynamics by piecewise linear systems. In the model of *Drosophila* circadian rhythms by Gonze, Goldbeter and colleagues [7] and in the generic genetic oscillator model of Vilar and colleagues, we showed that the dynamics can be reduced to studying two modes that dominate the system. Then, a piecewise linear approximation of the Gonze-Goldbeter model confirmed that the system is robust to sizable perturbations in initial conditions by describing large regions of stability around the limit cycle.

In circadian rhythms, as in many other biological applications, we are interested in understanding how or what in the system network is responsible for the robustness to both external and internal perturbations. Linearisation helps understand the system close to the limit cycle, including identifying which modes are dominant and how fast they converge to the limit cycle. Piecewise linear approximations show whether global regions of stability exist. Then by varying the system parameters or network configuration, one can examine how such changes affect the local and global stability. In this manner, we can explore both the vulnerabilities and the strategies for increasing robustness in oscillatory systems.

A Models

A.1 Model with regulatory feedback

A.1.1 Full model

The model considered here is taken from [7]:

$$
\begin{aligned}
\frac{dM_P}{dt} &= v_{sP}\frac{K_{IP}^n}{K_{IP}^n + C_N^n} - v_{mP}\frac{M_P}{K_{mP} + M_P} - k_d M_P \\
\frac{dP_0}{dt} &= k_{sP} M_P - V_{1P}\frac{P_0}{K_{1P} + P_0} + V_{2P}\frac{P_1}{K_{2P} + P_1} - k_d P_0 \\
\frac{dP_1}{dt} &= V_{1P}\frac{P_0}{K_{1P} + P_0} - V_{2P}\frac{P_1}{K_{2P} + P_1} - V_{3P}\frac{P_1}{K_{3P} + P_1} + V_{4P}\frac{P_2}{K_{4P} + P_2} - k_d P_1
\end{aligned}
$$

$$
\begin{aligned}
\frac{dP_2}{dt} &= V_{3P}\frac{P_1}{K_{3P}+P_1} - V_{4P}\frac{P_2}{K_{4P}+P_2} - k_3P_2T_2 + k_4C - v_{dP}\frac{P_2}{K_{dP}+P_2} - k_dP_2 \\
\frac{dM_T}{dt} &= v_{sT}\frac{K_{IT}^n}{K_{IT}^n+C_N^n} - v_{mT}\frac{M_T}{K_{mT}+M_T} - k_dM_T \\
\frac{dT_0}{dt} &= k_{sT}M_T - V_{1T}\frac{T_0}{K_{1T}+T_0} + V_{2T}\frac{T_1}{K_{2T}+T_1} - k_dT_0 \\
\frac{dT_1}{dt} &= V_{1T}\frac{T_0}{K_{1T}+T_0} - V_{2T}\frac{T_1}{K_{2T}+T_1} - V_{3T}\frac{T_1}{K_{3T}+T_1} + V_{4T}\frac{T_2}{K_{4T}+T_2} - k_dT_1 \\
\frac{dT_2}{dt} &= V_{3T}\frac{T_1}{K_{3T}+T_1} - V_{4T}\frac{T_2}{K_{4T}+T_2} - k_3P_2T_2 + k_4C - v_{dT}\frac{T_2}{K_{dT}+T_2} - k_dT_2 \\
\frac{dC}{dt} &= k_3P_2T_2 - k_4C - k_1C + k_2C_N - k_{dC}C \\
\frac{dC_N}{dt} &= k_1C - k_2C_N - K_{dC}C
\end{aligned}
$$

The parameters used (again, from [7]) are: $n = 4$, $v_{sP} = 1nMh^{-1}$, $v_{sT} = 1nMh^{-1}$, $v_{mP} = 0.7nMh^{-1}$, $v_{mT} = 0.7nMh^{-1}$, $v_{dP} = 2nMh^{-1}$, $v_{dT} = 2nMh^{-1}$, $k_{sP} = k_{sT} = 0.9h^{-1}$, $k_4 = 0.6h^{-1}$, $K_{mP} = K_{mT} = 0.2nM$, $K_{IP} = K_{IT} = 1nM$, $K_{dP} = K_{dT} = 0.2nM$, $K_{1P} = K_{1T} = K_{2P} = K_{2T} = K_{3P} = K_{3T} = K_{4P} = K_{4T} = 2nM$, $V_{1P} = V_{1T} = 8nMh^{-1}$, $V_{2P} = V_{2T} = 1nMh^{-1}$, $V_{3P} = V_{3T} = 8nMh^{-1}$, $V_{4P} = V_{4T} = 1nMh^{-1}$, $k_d = k_{dC} = k_{dN} = 0.01nMh^{-1}$.

A.1.2 Reduced model

This is the model used in section 2.2 to illustrate a piecewise linear approximation. In this simplification, $M_P = M_T$, $P_0 = T_0$, $P_1 = T_1$, $P_2 = T_2$, so the state variables are $M_P, P_0, P_1, P_2, C, C_N$.

$$
\begin{aligned}
\frac{dM_P}{dt} &= v_{sP}\frac{K_{IP}^n}{K_{IP}^n+C_N^n} - v_{mP}\frac{M_P}{K_{mP}+M_P} - k_dM_P \\
\frac{dP_0}{dt} &= k_{sP}M_P - V_{1P}\frac{P_0}{K_{1P}+P_0} + V_{2P}\frac{P_1}{K_{2P}+P_1} - k_dP_0 \\
\frac{dP_1}{dt} &= V_{1P}\frac{P_0}{K_{1P}+P_0} - V_{2P}\frac{P_1}{K_{2P}+P_1} - V_{3P}\frac{P_1}{K_{3P}+P_1} + V_{4P}\frac{P_2}{K_{4P}+P_2} - k_dP_1 \\
\frac{dP_2}{dt} &= V_{3P}\frac{P_1}{K_{3P}+P_1} - V_{4P}\frac{P_2}{K_{4P}+P_2} - k_3P_2^2 + k_4C - v_{dP}\frac{P_2}{K_{dP}+P_2} - k_dP_2 \\
\frac{dC}{dt} &= k_3P_2^2 - k_4C - k_1C + k_2C_N - k_{dC}C \\
\frac{dC_N}{dt} &= k_1C - k_2C_N - K_{dC}C
\end{aligned}
$$

A.2 Model with both regulatory and autocatalytic feedback

The following model is taken from [1]. The 7 state variables represent the concentrations of the activator genes D'_A, D'_R, the messenger RNA M_A, M_R, and the proteins A, R, C. The differential equations are given by

$$
\frac{dD'_A}{dt} = \gamma_A(1 - D'_A)A - \theta_A D'_A
$$

$$
\begin{aligned}
\frac{dD'_R}{dt} &= \gamma_R(1-D'_R)A - \theta_R D'_R \\
\frac{dM_A}{dt} &= \alpha_A + (\alpha'_A - \alpha_A)D'_A - \delta_{M_A}M_A \\
\frac{dA}{dt} &= \beta_A M_A + D'_A(\theta_A + \gamma_A A) + D'_R(\theta_R + \gamma_R A) - (\gamma_A + \gamma_R + \delta_A)A - \gamma_C AR \\
\frac{dM_R}{dt} &= \alpha_R + (\alpha'_R - \alpha_R)D'_R - \delta_{M_R}M_R \\
\frac{dR}{dt} &= \beta_R M_R + \delta_A C - \delta_R R - \gamma_C AR \\
\frac{dC}{dt} &= \gamma_C AR - \delta_A C
\end{aligned} \tag{3}
$$

The parameters used (again, from [1]) are: $\alpha_A = 50h^{-1}$, $\alpha'_A = 500h^{-1}$, $\alpha_R = 0.01h^{-1}$, $\alpha'_R = 50h^{-1}$, $\beta_A = 50h^{-1}$, $\beta_R = 5h^{-1}$, $\delta_{M_A} = 10h^{-1}$, $\delta_{M_R} = 0.2h^{-1}$, $\delta_A = 1h^{-1}$, $\delta_R = 0.2h^{-1}$, $\gamma_A = 1mol^{-1}hr^{-1}$, $\gamma_R = 1mol^{-1}hr^{-1}$, $\gamma_C = 2mol^{-1}hr^{-1}$, $\theta_A = 50h^{-1}$, and $\theta_R = 100h^{-1}$.

B Linearisation of Poincaré maps

The content of this appendix section is taken from [13]. Consider the nth-oder system

$$\dot{x} = f(x), \quad x(0) = x_0$$

with solution $\phi_t(x_0)$, i.e.,

$$\dot{\phi}_t(x_0) = f(\phi_t(x_0)), \quad \phi_0(x_0) = x_0 \tag{4}$$

Differentiate (4) with respect to x_0 to obtain

$$D_{x_0}\dot{\phi}_t(x_0) = D_x f(\phi_t(x_0))D_{x_0}\phi_t(x_0), \quad D_{x_0}\phi_0(x_0) = I \tag{5}$$

Define $\Phi_t(x_0) = D_{x_0}\phi_t(x_0)$. Then (5) becomes

$$\dot{\Phi}_t(x_0) = D_x f(\phi_t(x_0))\Phi_t(x_0), \quad \Phi_0(x_0) = I$$

which is the variational equation.

Consider a point $x_1 \in \mathbb{R}^n$ that is mapped by the flow to x_2 in T seconds, that is, $x_2 = \phi_T(x1)$. Choose an $(n-1)$-dimensional hyperplane S_1 that contains x_1 and that is transversal to the flow at x_1 (see Figure 8). Similarly, choose S_2 transversal to the flow at x_2.

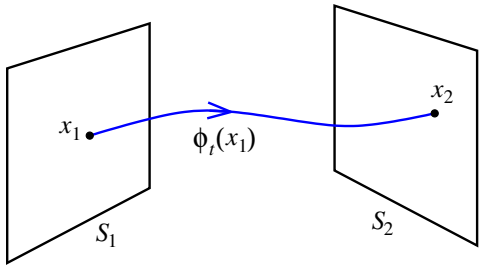

Figure 8: Generalised Poincaré map

The following results show that there exists a diffeomorphism $P_{S_1S_2}$ that maps a neighbourhood of x_1 on S_1 to a neighbourhood of x_2 on S_2, and then find an explicit expression for its derivative.

Note that the Poincaré map is defined as P_{SS}, basically by making $S_1 = S_2 = S$. The results also prove that the Poincaré map is a local diffeomorphism, and yields an expression for its derivative. The derivative is then used to show that given a fixed point x^* of a Poincaré map, the characteristic multipliers are a subset of the eigenvalues of $\Phi_T(x^*)$. Without loss of generality, move the origin to x_2. Let $C \in \mathbb{R}^{1\times n}$ be a vector orthogonal to S_2. Then $Cy = 0$ if and only if $y \in S_2$.

Lemma B.1 *There exists an open $U \in \mathbb{R}^n$ with $x_1 \in U$, and a unique C^1 map $\tau : U \to \mathbb{R}^n$, such that, for all $x \in U$, $\phi_{\tau(x)}(x) \in S_2$ and $\tau(x_1) = T$.*

Furthermore, it follows from the implicit function theorem that

$$D\tau(x_1) = \frac{-1}{Cf(x_2)} C'\Phi_T(x_1)$$

Lemma B.2 $f(x_2) = \Phi_T(x_1)f(x_1)$.

Definition B.1 *$P_{S_1S_2} : (U \bigcap S_1) \to S_2$ is the impact map, also known as the generalised Poincaré map, and is defined by*

$$P_{S_1S_2}(x) = \phi_{\tau(x)}(x)$$

Theorem B.1 *$P_{S_1S_2} : S_1 \to S_2$ is a local diffeomorphism at x_1 with*

$$DP_{S_1S_2}(x_1) = \left[I - \frac{1}{Cf(x_2)} f(x_2)C\right] \Phi_T(x_1)$$

Corollary B.1 *Let x^* be a fixed point of a Poincaré map P defined by a cross-section S, and let T^* be the period of the underlying limit cycle. Then $P = P_{SS}$, and*

$$DP(x^*) = \left[I - \frac{1}{Cf(x^*)} f(x^*)C\right] \Phi_{T^*}(x^*)$$

Theorem B.2 *Let x_1^* and x_2^* be any two points on a limit cycle. Let S_1 be an $(n-1)$-dimensional hyperplane passing through x_1^* transversal to $f(x_1^*)$. Likewise, define S_2 with respect to x_2^*. Then $DP_{S_1}(x_1^*)$ is similar to $DP_{S_2}(x_2^*)$.*

Corollary B.2 *As long as S is transversal to the limit cycle, the eigenvalues of $DP(x^*)$ are independent of the choice of x^*, and the position of S.*

Corollary B.3 *$f(x_1^*)$ is an eigenvector of $\Phi_{T^*}(x^*)$ with eigenvalue* 1.

Theorem B.3 *Let X^* be a fixed point of P, and let the eigenvalues of $\Phi_{T^*}(x^*)$ be $\{m_1, ..., m_{n-1}, 1\}$. Then, the eigenvalues of $DP(x^*)$ are $\{m_1, ..., m_{n-1}, 0\}$.*

C Piecewise linear systems

In this appendix, we briefly introduce piecewise linear systems (PLS). More details and results on analysis of limit cycles of PLS can be found in [6] and [5].

PLS are characterised by a set of affine linear systems

$$\dot{x} = A_i x + B_i \tag{6}$$

where $x \in \mathbb{R}^n$ is the state, together with a switching rule

$$i(x) \in \{1, ..., M\} \tag{7}$$

that captures discontinuous actions in the dynamics resulting from either the controller or system nonlinearities, and depends on present and possibly also on past values of x. By a solution of (6)-(7) we mean functions (x, i) satisfying (6)-(7), where $i(t)$ is piecewise constant. t is a *switching time* of a solution of (6)-(7) if $i(t)$ is discontinuous at t. We say a trajectory of (6)-(7) *switches* at some time t if t is a switching time. In the state space, switches occur at *switching surfaces* consisting of hyperplanes of dimension $n-1$

$$S_i = \{x |\ C_i x + d_i = 0\}$$

where C_i is a row vector and $i = \{1, ..., N\}$. Assume that existence of solution is always guaranteed for any initial condition. See [10] for conditions on existence of solutions for PLS.

Unlike linear systems that only have a single equilibrium point, PLS may exhibit multiple equilibrium points and/or limit cycles. Here, we are interested in limit cycles. For the remainder of this appendix, assume the PLS (6)-(7) has a limit cycle γ with period t^*, and that this limit cycle crosses transversely[1] k switching surfaces per cycle. For simplicity, and without loss of generality, assume the trajectory of the limit cycle evolves consecutively from system 1, to system 2, and so forth until it reaches system k and, finally, after completing one cycle, returns to system 1. Assume also the switching surfaces are ordered the same way (see Figure 9). This means the trajectory $\phi(t)$ of the limit cycle, starting at $x_1^* \in S_1$, satisfies $\phi(t_1^*) = x_2^* \in S_2$. Then system 2 "takes over" until $\phi(t_1^* + t_2^*) = x_3^* \in S_3$, and so on. The last affine linear system k takes the trajectory $\phi(t)$ from $x_k^* \in S_k$ back to $x_1^* \in S_1$, i.e., $\phi(t_1^* + t_2^* + \cdots + t_k^*) = x_{k+1}^* = x_1^* \in S_1$. Note that $t^* = t_1^* + t_2^* + \cdots + t_k^*$. Note also that there is no loss of generality in this characterisation of a limit cycle. If, for instance, the limit cycle crosses the same switching surface more than once, we simply have $S_i = S_j$ for some i, j. For convenience, indexes $k+1$ and 1 represent the same object, i.e., $x_{k+1}^* = x_1^*$, $S_{k+1} = S_1$, etc.

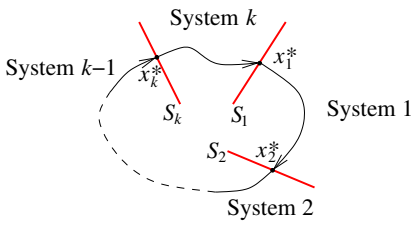

Figure 9: Limit cycle γ.

Conditions for the existence and local stability of limit cycles of PLS can be found in [5]. When a limit cycle γ is proven locally stable, then there exist a neighbourhood in S_1 around x_1^* such that any trajectory starting in this neighbourhood will converge asymptotically to the limit cycle γ. The next step is to characterise a reasonably large stable region around a locally stable limit cycle (see Figure 10). Such results can also be found in [5].

References

[1] José Vilar amd Hao Yuan Kueh, Naama Barkai, and Stanislas Leibler. Mechanisms of noise–resistance in genetic oscillators. *PNAS*, 99(9):5988–5992, 2002.

[1] ϕ is *transversal* to $S = \{x |\ Cx = d\}$ at $p = \phi(t) \in S$ if $C\dot{\phi}(t-0) \neq 0$. This is necessary or otherwise the limit cycle is unstable.

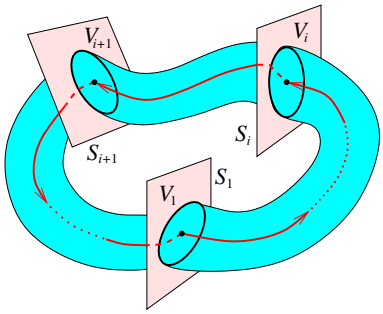

Figure 10: Region of stability around a limit cycle.

[2] N. Barkai and S. Leibler. Circadian clocks limited by noise. *Nature*, 403:267–268, 2000.

[3] J. C. Dunlap. Molecular bases for circadian clocks. *Cell*, 96:271–290, 1999.

[4] A. Goldbeter. *Biochemical Oscillations and Cellular Rhythms. The Molecular Bases of Periodic and Chaotic Behavior*. Cambridge, UK: Cambridge University Press, 1996.

[5] Jorge M. Gonçalves. Regions of stability for limit cycles of piecewise linear systems. Submitted for publication.

[6] Jorge M. Gonçalves, Alexandre Megretski, and Munther A. Dahleh. Global analysis of piecewise linear systems using impact maps and surface Lyapunov functions. *IEEE Transactions on Automatic Control*, 48(12):2089–2106, December 2003.

[7] Didier Gonze, José Halloy, Jean-Christophe Leloup, and Albert Goldbeter. Stochastic models for circadian rhythms: effect of molecular noise on periodic and chaotic behavior. *C. R. Biologies*, 326:189–203, 2003.

[8] Michael Hastings. Circadian clockwork: two loops are better than one. *Nature Reviews*, 1:143–146, November 2000.

[9] Michael Hastings, Akhilesh Reddy, and Elizabeth Maywood. A clockwork web: circadian timing in brain and periphery, in health and disease. *Nature Reviews*, 4:649–661, August 2003.

[10] J. Imura and A. van der Schaft. Characterization of well-posedness of piecewise-linear systems. *IEEE Transactions on Automatic Control*, 45(9):1600–1619, Sept 2000.

[11] Hassan K. Khalil. *Nonlinear Systems*. Prentice Hall, N.J., 2nd edition, 1996.

[12] J.-C. Leloup and A. Goldbeter. Modeling the molecular regulatory mechanism of circadian rhythms in *drosophila*. *BioEssays*, 22:84–93, 2000.

[13] Thomas Parker and Leon Chua. *Practical Numerical Algorithms for Chaotic Systems*. Springer-Verlag, 1989.

[14] Pablo A. Parrilo. *Structured Semidefinite Programs and Semialgebraic Geometry Methods in Robustness and Optimization*. PhD thesis, California Institute of Technology, Pasadena, CA, 2000.

[15] S. M. Reppert and D. R. Weaver. Molecular analysis of mammalian circadian rhythms. *Annu. Rev. Physiol.*, 63:647–676, 2001.

[16] S. Strogatz. *Sync: The emerging science of spontaneous order*. New York: Hyperion, 2003.

[17] J. A. Williams and A. Sehgal. Molecular components of the circadian system in *drosophila*. *Annu. Rev. Physiol.*, 63:729–755, 2001.